Appendix for

TOR acts as a metabolic gatekeeper for auxin-dependent lateral root initiation in *Arabidopsis thaliana*

Michael Stitz, David Kuster, Maximilian Reinert, Mikhail Schepetilnikov, Béatrice Berthet, Jazmin Reyes-Hernández, Denis Janocha, Anthony Artins, Marc Boix, Rossana Henriques, Anne Pfeiffer, Jan Lohmann, Emmanuel Gaquerel and Alexis Maizel

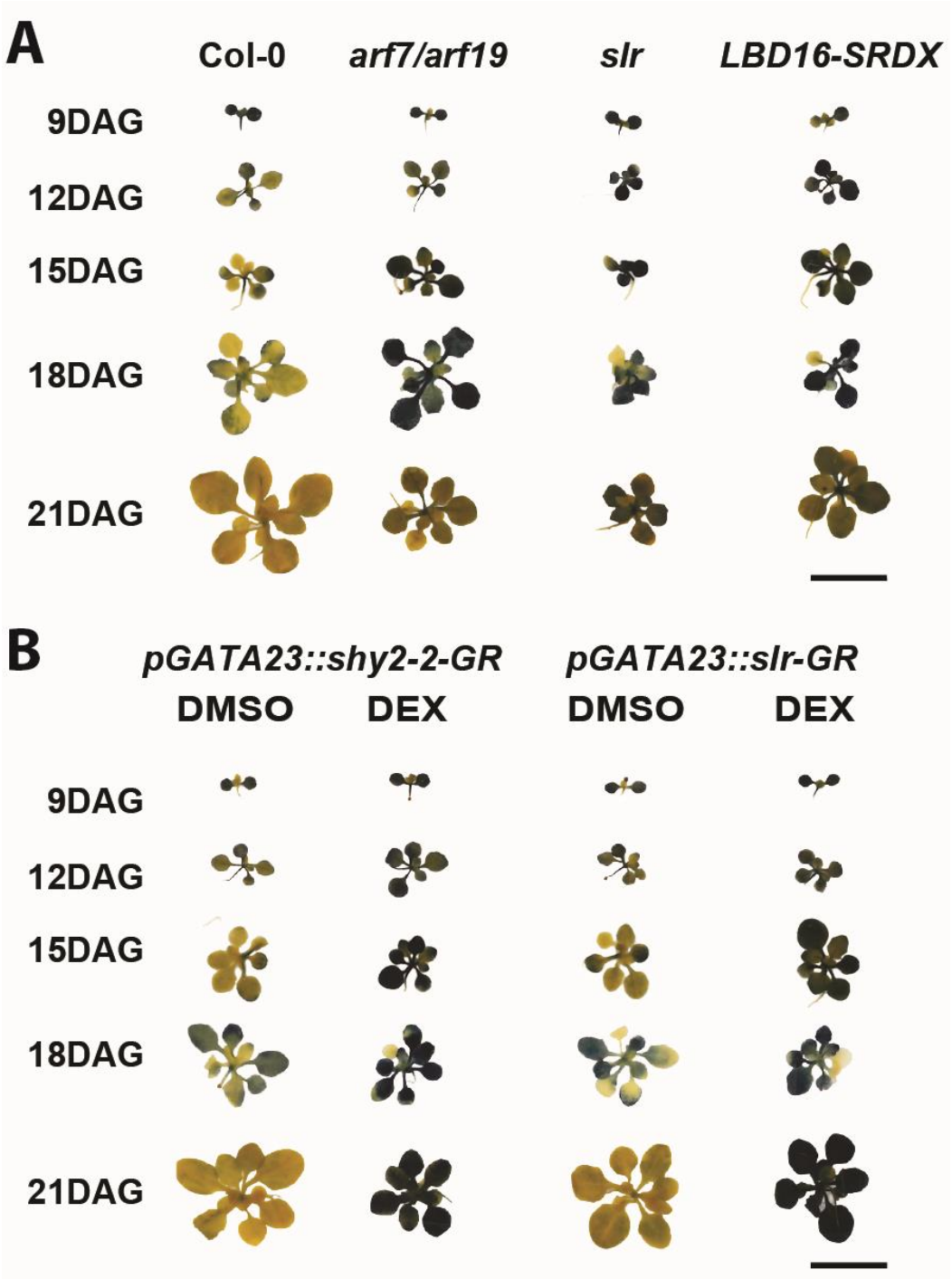

Appendix Figure S1. Lateral root deficiency leads to starch hyperaccumulation in leaves.

A. Representative images of rosettes of seedlings stained with a Lugol's Iodine solution for starch accumulation at the indicated day after germination (DAG) in Col-0, *arf7/arf19, slr,* and *gLBD16-SRDX.*

B. In the inducible lateral rootless lines, *pGATA23::shy2-2-GR* and *pGATA23::slr1-GR* grown on control medium (DMSO) starch staining resemble Col-0, while those devoid of LRs grown on Dexamethasone (DEX, 10µM) show the intense starch staining observed for LR-less mutants in (A) from the 9 to 21 DAG. Scale bar: 1 cm.

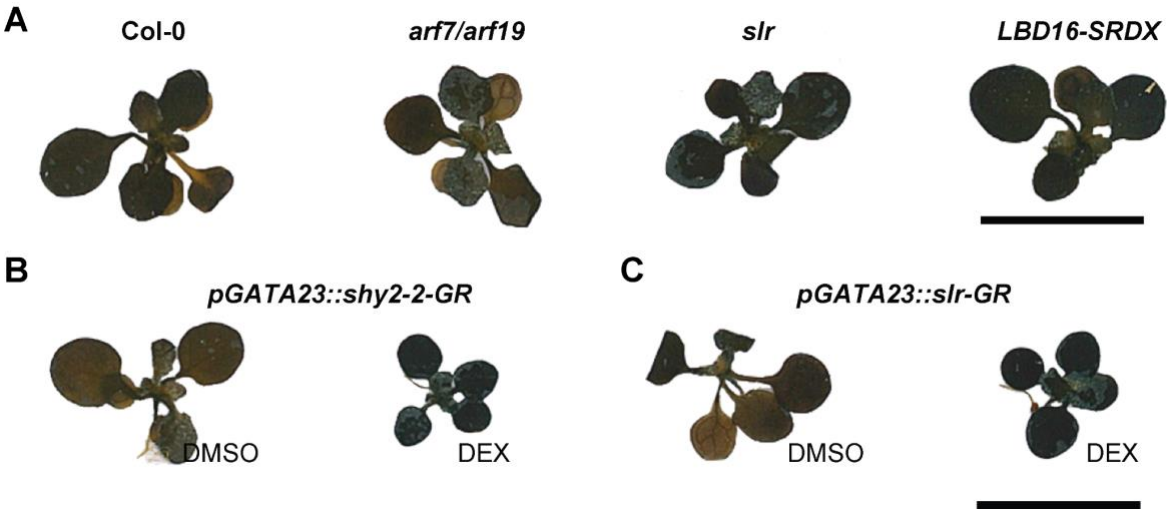

Appendix Figure S2. Comparable starch content in foliage at the end of the light period in plants producing LR or not.

A. Representative scanning images of rosettes of seedlings stained with a Lugol's Iodine solution for starch accumulation 15 days after germination (DAG) at the end of the light phase in Col-0, *arf7/arf19, slr,* and *gLBD16-SRDX.*

B. In the inducible lateral rootless lines, *pGATA23::shy2-2-GR* and *pGATA23::slr1-GR* grown on DMSO control medium or grown on 10µM Dexamethasone (DEX, 10µM. show comparably intense starch staining as observed for LR-less mutants and Col-0 in (A). Scale bar: 1 cm.

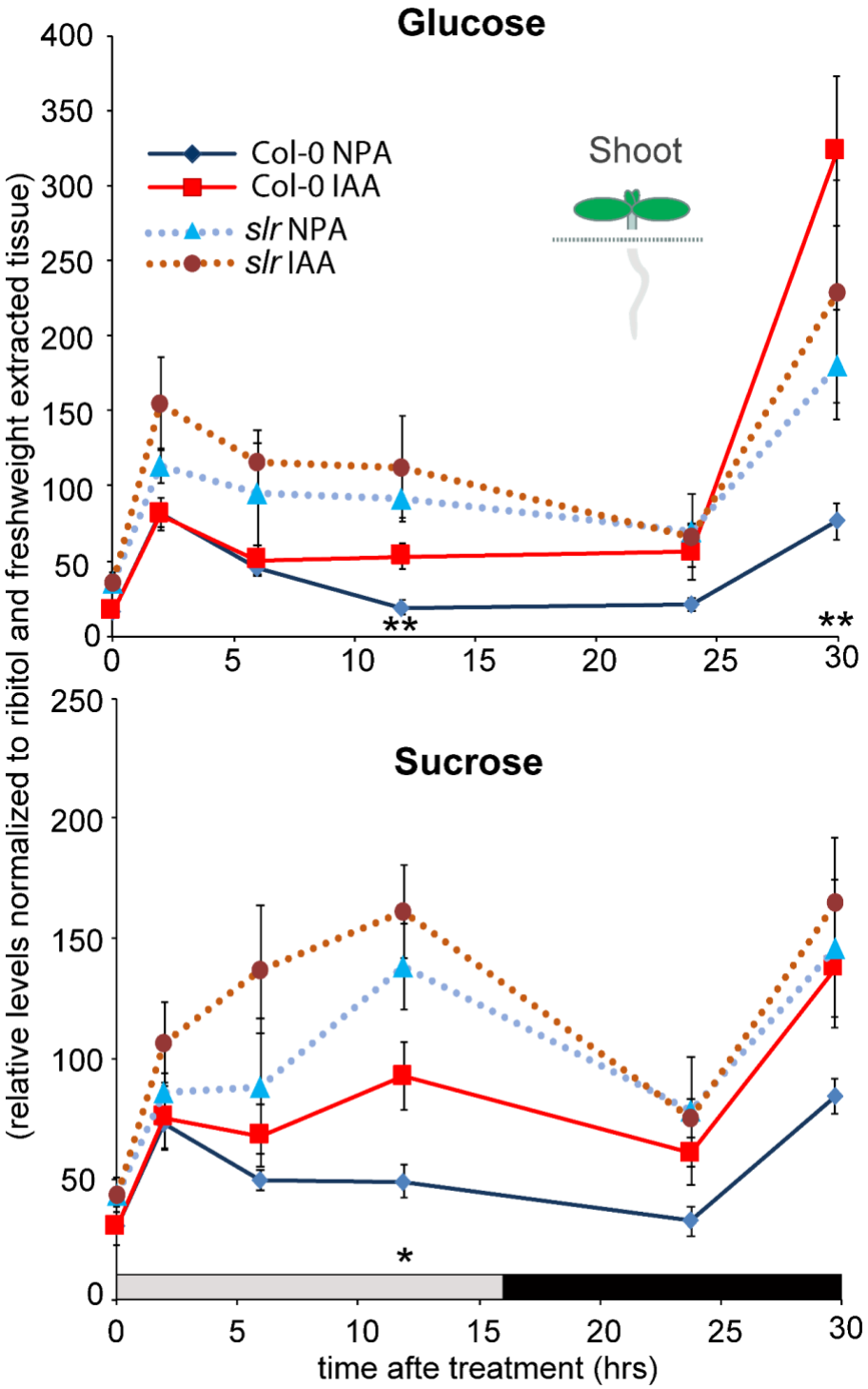

Appendix Figure S3. Glucose and Sucrose levels in shoots of IAA-treated Col-0 and *slr* seedlings.

The plots depict the levels of glucose and sucrose in shoot tissues of Col-0 (solid lines) and *slr* (dashed lines) at the indicated time after IAA application. Values are means (± SE, *n*=5 biological replicates) of relative levels normalized to the ribitol internal standard and per mg fresh weight. Asterisks indicate significant differences between NPA-treated control conditions and auxin (IAA) induced root tissues (unpaired t-test; * = $p < 0.05$, ** = $p < 0.001$). The shoot metabolomics data are summarised in File EV1.

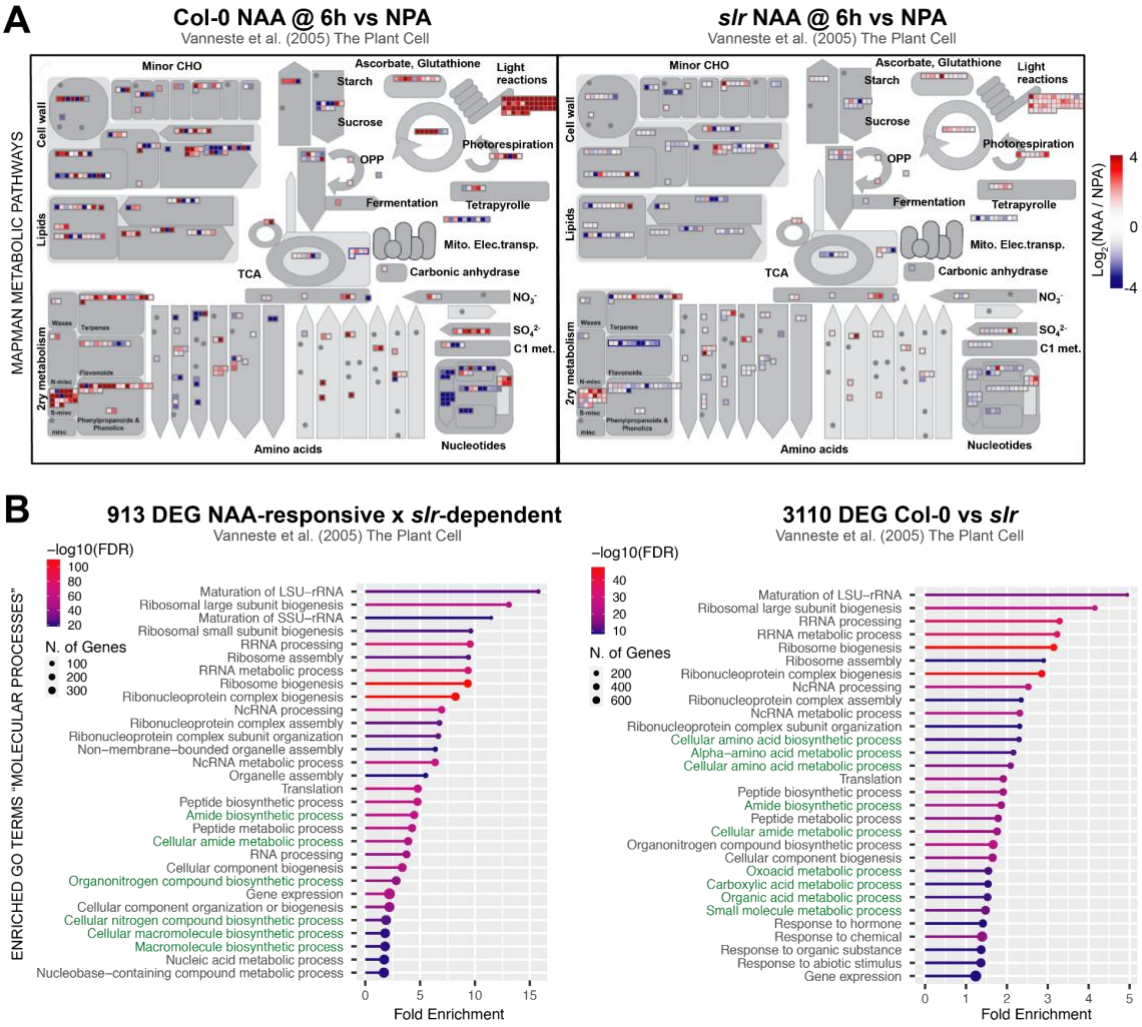

Appendix Figure S4. Auxin/*slr*-dependent signaling reconfigures the carbon metabolism-related transcriptome during LR formation is influenced.

A. MAPMAN-based overview of fold-change (log_2-transformed) reconfigurations of central carbon metabolism-related transcripts from root segments of Col-0 and *slr* mutant seedlings after 6h of transfer from NPA to the auxin analog NAA (α-naphthaleneacetic acid).

B. DEG sets for the comparison of overall Col-0 vs. *slr* root transcriptomes (right panel) and specifically associated with an interactive NAA x *slr* effect (left panel) were extracted from the VisuaLRTC transcriptome/statistical data compendium by Parizot *et al.* (2010). Enrichment analyses for Molecular Processes GO terms were conducted using ShinyGO v0.75 (Ge *et al.*, 2019) with an FDR P-value cutoff of 0.5 and a maximum number of top pathways to show 30. Central carbon metabolism-related GO terms are highlighted in green. Original transcriptomics data for both analyses are from Vanneste *et al.* (2005) pioneer exploration of auxin-/*slr*-dependent root transcriptomics responses during synchronized LR induction.

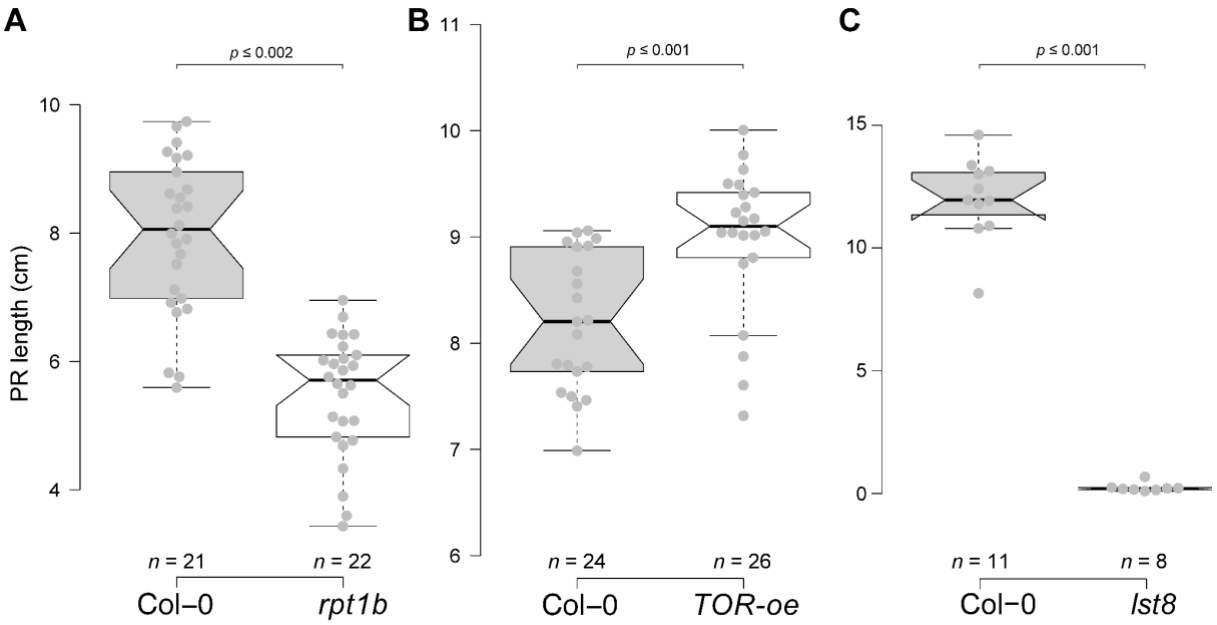

Appendix Figure S5. TOR over-activation leads to longer primary roots, whereas impairment of the TOR machinery results in reduced primary root length.

A. 14-day-old TOR-oe seedlings (GK548) show significantly longer primary roots than Col-0 ($p \leq 0.002$) when grown on ½ MS media containing 110mM Sucrose. (unpaired *t*-test).

B. 14-day-old *rpt1b* seedlings show significantly shorter primary roots than Col-0 ($p \leq 0.001$).

C. *lst8* seedlings at 18 DAG show strongly impaired primary root growth. (unpaired *t*-test)

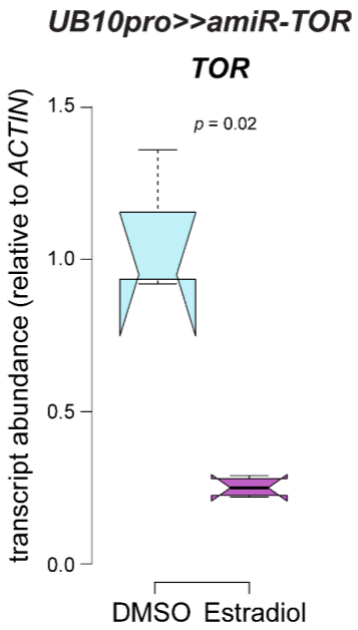

Appendix Figure S6. *TOR* silencing in *UB10pro>>amiR-TOR*

Root tissues of *UB10pro>>amiR-TOR* plants grown for 24 h on ½ MS media containing 10 µM ß-Estradiol have significantly lower TOR-mRNA levels than *UB10pro>>amiR-TOR* control plants grown for 24 h on ½ MS media containing DMSO control solution (*n*=4 biological replicates, unpaired *t*-test).

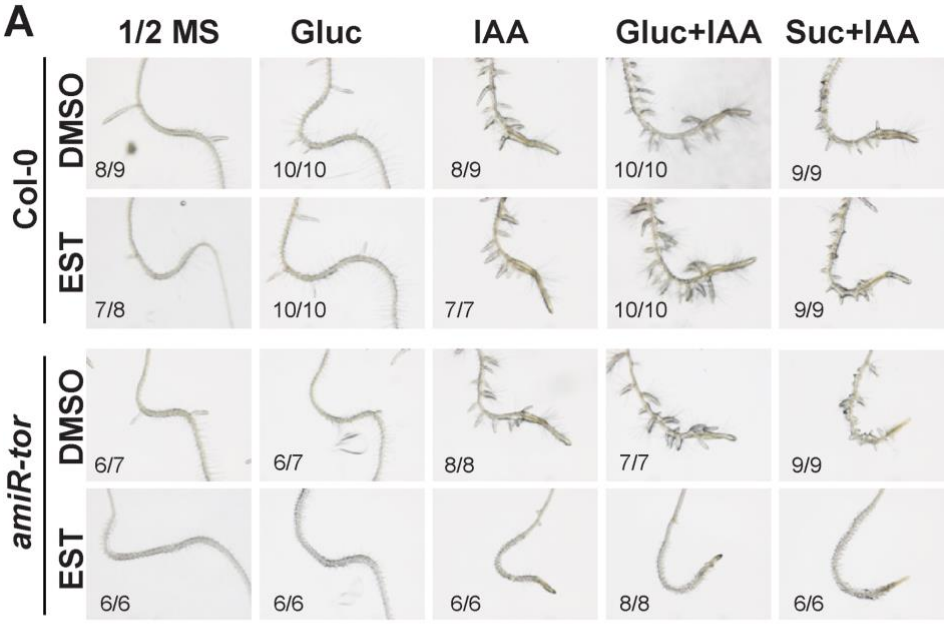

B

Percentage of Rootbends producing LR

	Col-0		*amiR-tor*	
Treatment	**DMSO**	**EST**	**DMSO**	**EST**
1/2 MS	86	88	86	0
Gluc	100	100	86	0
IAA	100	100	100	0
Gluc+IAA	100	100	100	0
Suc+IAA	100	100	100	0

Appendix Figure S7. IAA or external carbohydrate sources in TOR-deficient seedlings can not rescue lateral root formation.

A. Representative images of Col-0 and *UB10pro>>amiR-TOR* roots after 72h after rescue with 2% Glucose, 10 µM IAA, 2% Glucose + 10 µM IAA, or 2% Sucrose + 10 µM IAA. Before transfer to the rescue media, seedlings were pre-treated for 24h with either DMSO or 10 µM ß-Estradiol.

B. Quantification of the LR-rescue in UB10pro>>amiR-TOR seedlings.

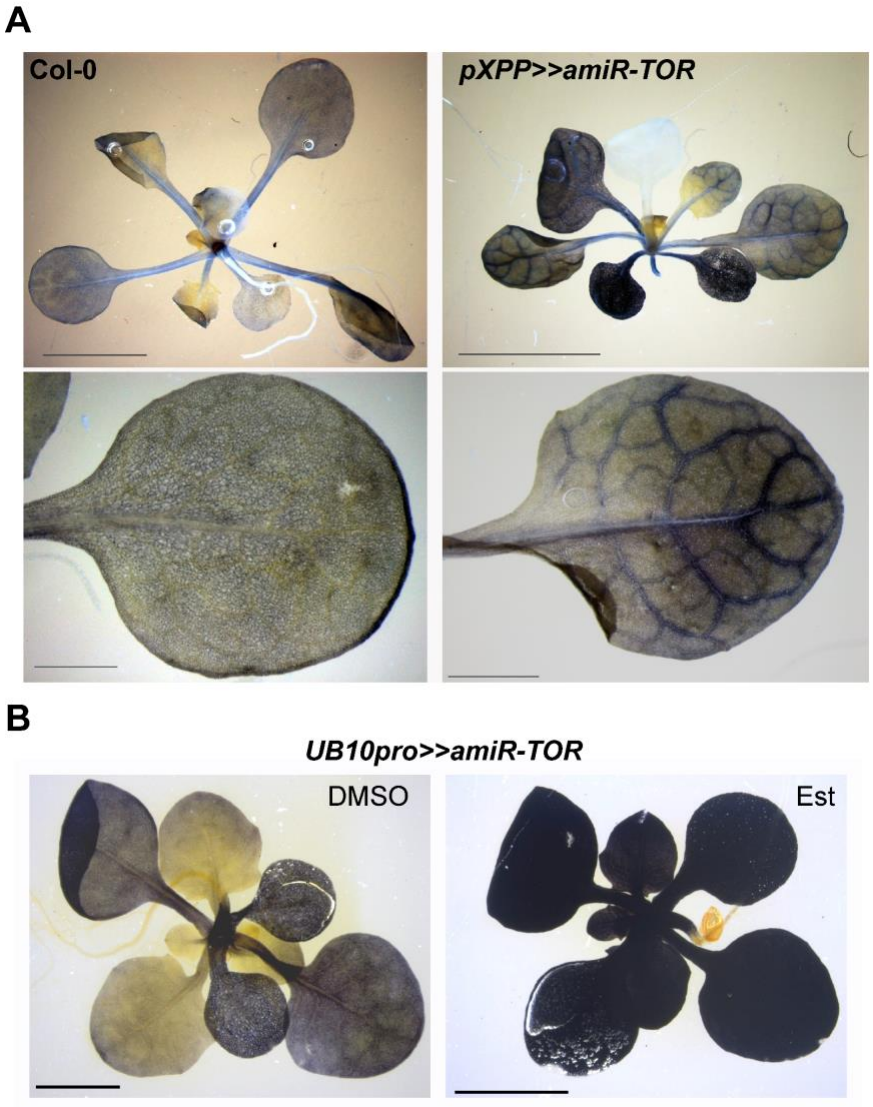

Appendix Figure S8. Foliar accumulation of starch upon TOR silencing.
A. Starch staining in leaves of the *pXPP>>amiR-TOR* line. 12 DAG seedlings of *pXPP>>amiR-TOR* plants grown on DEX for 48h specifically accumulate starch in the vasculature of leaves. Scale bars: upper panel: 5mm, lower panel: 1 mm).
B. Starch staining in leaves of the *UB10pro>>amiR-TOR* line. 14DAG *UB10pro>>amiR-TOR* plants grown for 48hrs on Estradiol accumulate starch throughout the foliage, compared to DMSO-grown controls.

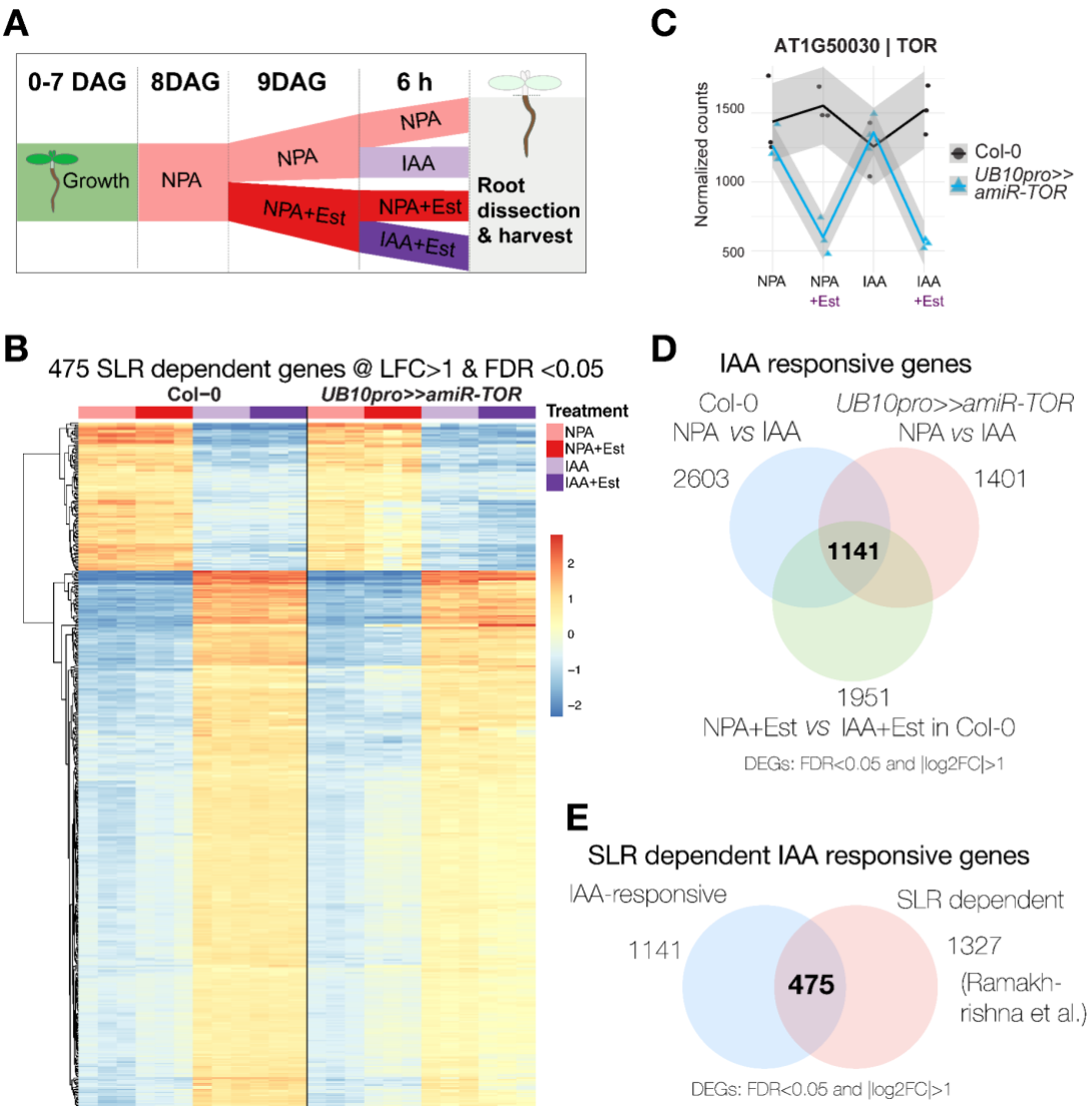

Appendix Figure S9. Transcriptome analysis upon auxin-induced induction of lateral root formation in *UB10pro>>amiR-TOR*.

A. Schematic depicting how samples for this RNA-seq data set were prepared.

B. Heatmap from a hierarchical clustering analysis (HCA) showing z-score normalized relative levels of 475 SLR-dependent genes in tissues +/- induced for LR-formation, and +/- induced for TOR-knockdown (One-way ANOVA, LFC>1 & FDR <0.05)

C. Extracted traces for RNAseq sample set shows reduction of TOR transcripts in samples generated from UB10pro>>amiR-TOR roots grown on Est containing media compared to control and Col-0 samples.

D. Venn-diagram of IAA-responsive genes with log 2-fold change >1 f commonly and differentially expressed in Col-0 and *UB10pro>>amiR-TOR* after shifting from NPA to 10 µM IAA, and Col-0 after the shift from NPA and Est to IAA and Est.

E. Venn diagram showing IAA-responsive genes commonly and differentially expressed in Col-0 and *UB10pro>>amiR-TOR* 6h and Col-0 after the shift from NPA and Est to IAA and Est.

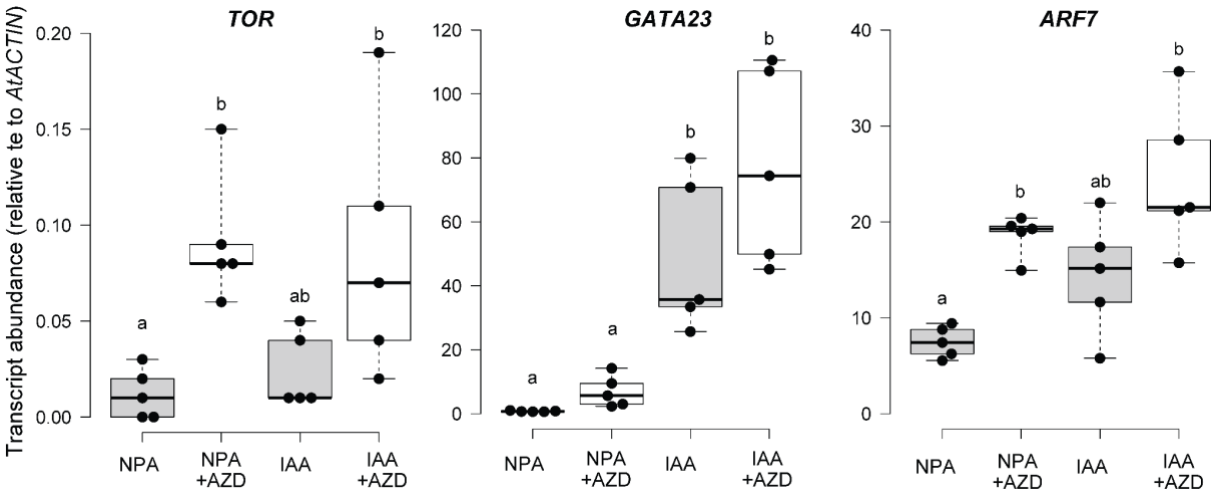

Appendix Figure S10. Expression of TOR, GATA23, and ARF7 transcripts upon inhibition of TOR via AZD8055.

TOR's relative expression levels (normalized to ACTIN) are increased by AZD8055, while GATA23 and ARF7 are not reduced by TOR inhibition. Comparison between samples was performed by one-way ANOVA. Different letters indicate significant differences based on a posthoc Tukey HSD Test (α = 0.05), n=5 biological replicates.

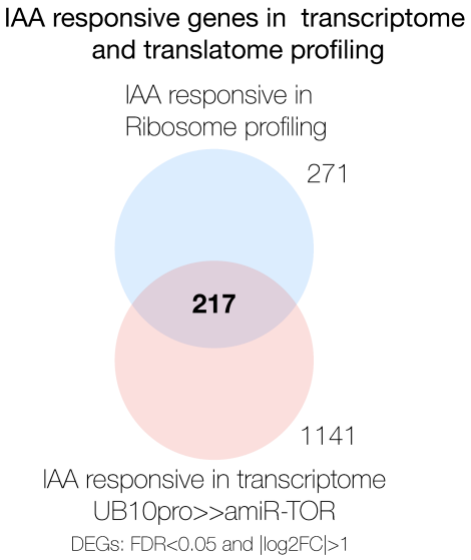

Appendix Figure S11. IAA-responsive genes detected during ribosome profiling and TOR inhibition IAA induced in the RNA-seq experiment under TOR deficiency vastly overlap. Venn-diagram showing IAA-responsive genes commonly and differentially expressed 6h of IAA application in Col-0 after previous AZD8055 inhibition of TOR and *UB10pro>>amiR-TOR* on Est.

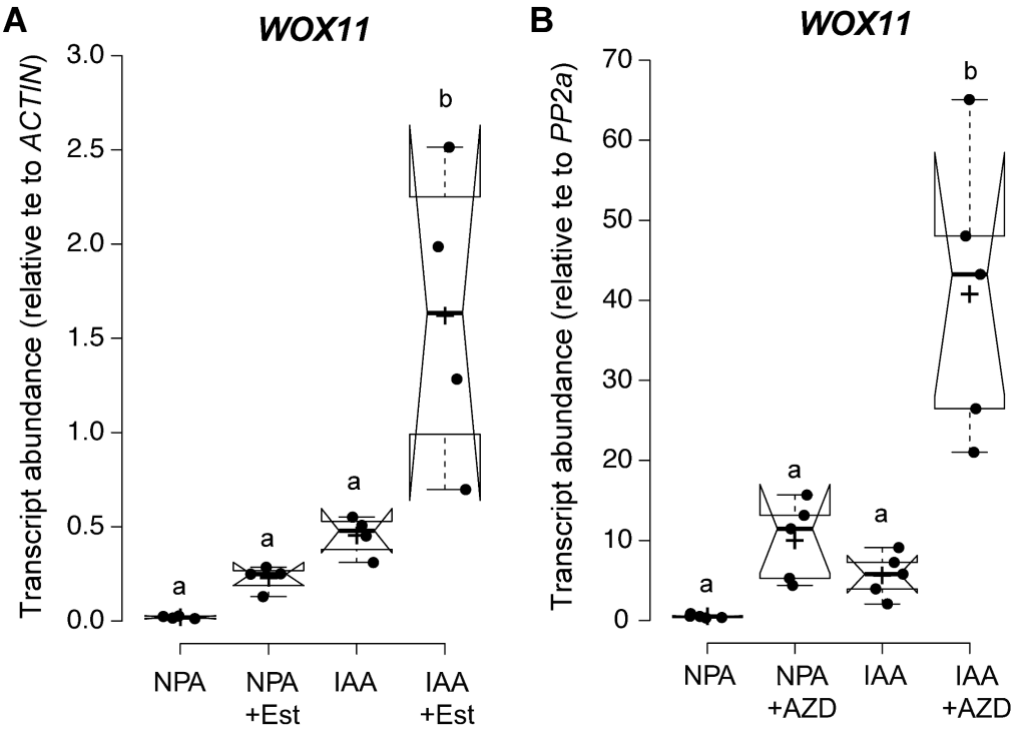

Appendix Figure S12. *WOX11* expression upon TOR-knockdown or TOR inhibition.
The abundance of WOX11 transcripts is increased 6hrs after LR induction by 10µM IAA in RT-q-PCR samples of *UB10pro>>amiR-TOR* after TOR-knock-down (A) as well as in Col-0 samples after TOR-inhibition by 10 µM AZD8055 (B). Comparison between samples was performed by one-way ANOVA. Different letters indicate significant differences based on a post-hoc Tukey HSD Test (α = 0.05, A, *n*=3; B, *n*=4; C, *n*=5 biological replicates).